Phonon modes and vibrational entropy of disordered alloys with short-range order: A first-principles calculation

Aftab Alam

Department of Materials Science and Engineering, University of Illinois, Urbana-Champaign, Illinois 61801, USA

Rajiv Kumar Chouhan and Abhijit Mookerjee

Advanced Materials Research Unit and Department of Materials Science, S. N. Bose National Center for Basic Sciences, JD Block, Sector III, Salt Lake City, Kolkata 700 098, India

(Received 12 October 2010; revised manuscript received 9 December 2010; published 3 February 2011)

There has been increasing evidence about the effects of short-range order (or local chemical environment effects) on the lattice dynamics of alloys, which eventually affect the vibrational entropy difference among various phases of a compound, and hence their relative stability. In this article, we present an *ab initio* calculation of the lattice dynamics and the vibrational entropy of disordered systems with short-range order. The features in the phonon density of states were found to change systematically with chemical short-range order in the alloy. Plausible explanations for our smaller value of vibrational entropy of mixing compared to experiment are given in some detail. A general trend of the magnitude of vibrational entropy of mixing is explained by making a connection to the phonon lifetime broadening, an intrinsic property of any multiple scattering phenomenon. We illustrate the method by applying it to a body-centered cubic $Fe_{1-x}Cr_x$ alloy.

DOI: 10.1103/PhysRevB.83.054201 PACS number(s): 63.20.dk, 63.50.Gh, 65.40.−b

I. INTRODUCTION

An accurate and reliable estimate of lattice vibrational effects is a long-standing problem for first-principles calculations of substitutional alloy thermodynamics. This is mainly due to the more complicated nature of the phonon problem, with the existence of an essential off-diagonal disorder in the dynamical matrix. Moreover, the sum rule obeyed by the diagonal and off-diagonal parts of the force constants leads to the so-called environmental disorder.[1] The problem becomes even more difficult if the vibrational properties of the concerned alloy are sensitive to the short-range features of atomic arrangements. One is then required to provide a conditional configuration averaging scheme for the disordered alloy which captures the effect of correlated, and not simply homogeneous, disorder. Typically, the ranges of interatomic force constants are not much larger than those of the interatomic distances. There have been no detailed first-principles investigations of how the phonon density of states (DOS) depends on short-range ordering (or local atomic configuration) in alloys. In addition, since the phonon DOS is a key quantity for any understanding of vibrational entropy (at least in the harmonic approximation), such a dependence on short-range ordering (SRO) is implicitly hidden in the entropy as well. Keeping in mind a growing effort to understand the reasons behind the vibrational entropy differences between various states of materials,[2,3] we formulate a new method which can take into account the effect of the local chemical environment on the lattice dynamics of disordered alloys and hence provide a deeper insight into the understanding of the origin of such entropy differences. Within the experimental framework, there have been several advances made in this direction. The experimental literature mainly relies on three basic techniques, namely, differential calorimetry,[3,4] inelastic neutron scattering,[5] and nuclear resonant inelastic x-ray scattering.[6] Of these the nuclear resonant scattering experiment seems quite promising. Some of the applications of this method provide a better understanding of the microstructure of alloys by assigning the dependence of the local chemical environment on the phonon DOS.[7] Although there are numerous experimental studies in this area, a complete theoretical understanding is still lacking. This situation has motivated a few theoretical studies,[8–10] which have addressed properties that are sensitive to the presence of short-range ordering in alloys. However, to our knowledge, these studies are either limited to model systems or based on the use of a separate *ab initio* energetics and interatomic potentials. It is therefore required to have a direct first-principles calculation of the lattice dynamics and the vibrational entropy of disordered alloys with short-range order.

Challenged by this possibility and motivated by a lack of available knowledge, we present a generalized method to investigate the vibrational properties of disordered alloys with SRO. This method should explicitly take into account the fluctuation in masses, scattering length (diagonal disorder), and force constants (off-diagonal disorder). The generalization should in principle allow the method an extra capability of capturing the effect of correlated disorder arising out of SRO. This technique is based on the augmented space theorem suggested by one of us[11] combined with the recursion method of Haydock *et al.*[12] to obtain the conditional configuration averaged Green's function. Unlike the *virtual crystal approximation* (VCA) and the *coherent potential approximation* (CPA)[13] (single-site approximation), the present formalism can take into account multisite disorder effects. Although generalizations of the CPA[14] exist in the literature, most of these either are limited to very special types of off-diagonal disorder or violate the lattice translational symmetry and Herglotz analytic properties of the configuration averaged Green's function. Of such various methods, one approach has emerged to be somewhat promising, namely, the nonlocal coherent potential approximation (NL-CPA).[15]

 ©2011 American Physical Society

Keeping in mind the increasing interest in investigating the role of phonon entropy on the thermodynamic stability of a compound, we choose a technologically important alloy system, Fe-Cr. The phase diagram of Fe-Cr at high temperatures includes a body-centered cubic (bcc) single-phase region over a broad range of composition, with a σ-phase region near equiatomic compositions from 725 to 1103 K. Experimental observations in the temperature range 675–773 indicate that chemical unmixing occurs homogeneously by a mechanism like spinodal decomposition.[16] In fact Fe-Cr alloys constitute the basic ingredient of stainless steel that for a century has been one of the most important structural materials, and hence some properties of stainless steel are inherited from this parent alloy.

In Fe-Cr alloys the dominant disorder is in the dynamical matrices. The single-site mean-field approaches cannot describe off-diagonal disorder properly, hence the importance of the Augmented Space Recursion (ASR) calculation. In an earlier paper[17] we have studied the effect of strong mass disorder leading to resonances in NiPt alloys. In this paper we shall focus on strong off-diagonal disorder. The concerned study is based on the phonon DOS and vibrational entropy of mixing of bcc Fe-Cr. We also analyze for the effects of SRO on these lattice dynamical properties, which in turn are related to the thermodynamics of the alloy.

Various mechanisms have been suggested from time to time to explain the origin of vibrational entropy differences in alloys. Some of them are the *bond proportion* effect,[18] the *volume* effect, the *size mismatch* effect,[19] and so on. The entropy difference is actually related to the difference in the phonon DOS between the two concerned states. An intrinsic quantity from which this phonon DOS is obtained in most of the theoretical calculations is the phonon dispersion. In disordered alloys, this dispersion is associated with a full width at half maximum (FWHM), which provides finite lifetime broadening to phonon scattering. Considering this quantity to be one of the most basic quantities in any phonon theory of disordered alloys, we intuitively connect it to explain a general trend of the magnitude of vibrational entropy difference.

In contrast to previous semiemperical calculations[9] and experiments,[5,20] we found a comparatively smaller value of the phonon entropy of mixing. We provide plausible explanations for the comparatively large value of vibrational entropy difference obtained in previous studies. While this result does not rule out the possibility that lattice vibrations play a significant role in other systems, it does point out that vibrational effects in Fe-Cr may be comparatively smaller than originally claimed.

In the remainder of this paper, we first describe a generalized formalism (in Sec. II) which can take into account the effect of SRO on the phonon DOS and vibrational entropy differences. Although the original augmented space theorem (related to phonon problem) was quoted in Ref. 17, its generalization is nontrivial. Section III is devoted to various computational details. The results of these calculations, describing the physical origin of unexpected lattice dynamics of the Fe-Cr alloy, are discussed in Sec. IV. The mechanism we identify is unlikely to be limited to the Fe-Cr system alone and points to an important feature that needs to be accounted for in order to properly model the local chemical environmental effect in any alloy system to accurately predict vibrational entropy. Concluding remarks are presented in Sec. V.

II. METHODOLOGY

Since the augmented space method has been described in great detail in many earlier papers, we introduce here only those salient points which are of direct relevance to our generalization to SRO for the phonon problem. Interested readers are referred to the Refs. 17 and 21 for further details.

In order to maintain consistent notations, we first provide in brief the mathematics for uncorrelated disorder (or homogeneous disorder) and then proceed for the generalization to the correlated disorder problem (arising out of SRO). For the sake of visualization, we also explain the corresponding physical phenomenon, which these theories actually capture, in terms of the multiple scattering picture.

A. Multiple scattering phenomenon

When a phonon propagates in a random alloy, it encounters irreducible multiple scatterings both repeatedly off single local configuration fluctuations and successively off simultaneous fluctuations on different sites. As mentioned in the Introduction, being a single-site mean-field approximation CPA takes into account only the single, local fluctuations. This is shown in the left panel of Fig. 1, which is a two-dimensional cartoon diagram of the multiple scattering phenomenon captured by the CPA. The black circle is a single fluctuation site embedded in an average medium denoted by light circles. Within the CPA (diagonal disorder), the irreducible scattering by the defect is confined to the defect site itself. The (red) box around the fluctuation site indicates the region of influence of the perturbation. This is an oversimplified model of the phonon problem for disordered alloys, since none of the springs are affected by the presence of this defect and the force constants are the same everywhere. In other words, the averaging is done over all possible occupations of single sites only. The right panel in Fig. 1 illustrates the multiple scattering phenomenon captured within our augmented space method.

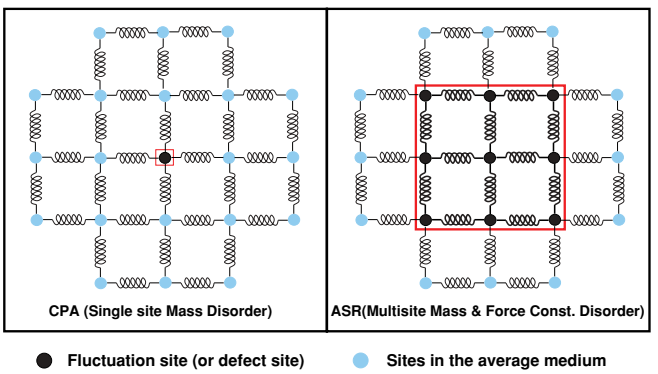

FIG. 1. (Color online) Multiple scattering picture for the single-site CPA, and the multisite ASR. The black circles indicate the fluctuation site and the red square box around them indicates the region of influence. Within the CPA the effect of fluctuation is limited to the single site itself; however ASR takes into account the influence of neighboring sites as well.

One can easily see the difference as compared to the CPA. In this picture, the main difference is the region of perturbation which is not only the site of fluctuation but also its neighboring environment. The box around the dark circles shows the region of influence, which is an example of a model including the effect of the second nearest neighbor environment. One can perform calculations for further extended neighbors as well. During the process of propagation, the phonon at the fluctuation site scatters from all of its neighbors, and their force constants also undergo fluctuations (indicated by thick spring lines in contrast to the thin ones for the average medium). In fact, the whole cluster of atoms [within the red box] undergoes fluctuations both in masses (diagonal disorder) and force constants (off-diagonal disorder). This is an example of homogeneous disorder. Another thing to notice is the way scattering is spread all over the lattice, although the strength of scattering decreases with distance because of the short-range nature of phonon interaction. Apart from the fluctuations in masses and force constants, the scattering lengths of the alloy components might be very different from one another. For the sake of completeness, we have also included fluctuations in scattering lengths.

B. Phonons with short-range order

The augmented space formalism for correlated disorder has been derived and discussed before for the electronic problem.[22] In this section, we present a generalization of the same to the phonon problem and hence relate it to the phonon DOS and vibrational entropy. We first present the salient features of the method for homogeneous disorder and then discuss its generalization to correlated disorder.

The basic idea behind the augmented space method for configuration averaging is to extend the usual real Hilbert space $\mathcal{H}$ to include a configuration space $\mathbf{\Psi}$. Disorder fluctuations are described in $\mathbf{\Psi}$. Suppose $\{n_R\}$ to be a collection of discrete independent random variables and $F(\{n_R\})$ to be some function of these variables. If each random variables n_R takes on values $\{m_1,m_2,\ldots,m_r,\ldots\}$ one can decompose the joint probability distribution function of these variables $P(\{n_R\})$ as

$$P(n_1,n_2\ldots,n_r,\ldots) = p_1(n_1)\ p_2(n_2)\ldots p_r(n_r)\ldots$$

Each p_i is positive definite and has finite moments to all orders. A Hilbert space Ψ_R (spanned by the states of n_R) is constructed for each density p_R, and the full system configuration space is defined as $\mathbf{\Psi} = \prod_R^{\otimes} \Psi_R$. A self-adjoint operator $N_R \in \Psi_R$ is associated with each random variable n_R, such that

$$p_R(n_R) = -\frac{1}{\pi}\lim_{\delta\to 0} \Im m\left\langle \nu_0^R\right| [(n_R + i\delta)I - N_R]^{-1}\left|\nu_0^R\right\rangle, \qquad (1)$$

where $|\nu_0^R\rangle = \sum_{j=1}^{\alpha} w_j |m_j^R\rangle$ is a specific member of Ψ_R. The ground state $|\nu_0\rangle$ in the full product space Ψ is defined as $|\nu_0\rangle = \prod_R^{\otimes} |\nu_0^R\rangle$.

According to augmented space theorem, the configuration average of $F(\{n_R\})$ is

$$\langle\langle F\rangle\rangle = \langle\nu_0|\ \widetilde{F}(\widetilde{N}^{(1)},\widetilde{N}^{(2)},\ldots,\widetilde{N}^{(r)},\ldots)|\nu_0\rangle,$$

where

$$\widetilde{N}^{(R)} = I\otimes\cdots\otimes N_R\cdots\otimes I\otimes\cdots \qquad (2)$$

and $\widetilde{F}$ is the same function of $\widetilde{N}^{(R)}$ as F was of $n_R s$. The calculation of the configuration average $\langle\langle F\rangle\rangle$ thus reduces to the problem of obtaining the above expectation value.

However if the random variables $\{n_R\}$ are correlated (instead of being independent), then the joint probability distribution should be decomposed as

$$P(n_1,n_2\ldots,n_r,\ldots) = p_1(n_1)\ p_2(n_2|n_1)\ p_3(n_3|n_1,n_2)\ldots \qquad (3)$$

And in general for a correlated variable n_R, one has an associated operator,

$$\widetilde{N}^{(R)}_{\rm corr} = \sum_{l_1}\cdots\sum_{l_{R-1}} P_1^{l_1}\otimes P_2^{l_2}\otimes\cdots\otimes N_R^{l_1,\ldots,l_{R-1}}\otimes I\otimes\cdots, \qquad (4)$$

where the operator $N_R^{l_1,\ldots,l_{i-1}}$ is associated with the conditional probability density $p_i(n_i|n_1,n_2,\ldots,n_{i-1})$ and $P_i^{l_i}$ are projection operators on a specific state l_i. The elegance of the formulation is that the basic augmented space theorem still holds rigorously, but $\widetilde{N}(R)$, instead being of the form given by Eq. (2), now has the form of Eq. (4).

For a binary alloy, the macroscopic state of order is described in terms of the Warren-Cowley short-range order parameter,

$$\alpha_R^{AB} = 1 - \frac{P_R(B|A)}{y},$$

where the center of the Rth shell is occupied by A atom, y denotes the macroscopic concentration of species B, and P_R is the probability of finding a B atom anywhere in the Rth shell centered around an A atom.

In terms of the above-defined SRO parameter, the probability densities associated with the sites belonging to first nearest neighbor shell are given by

$$\begin{aligned} p\left(n_{R_2}\middle|n_{R_1}=1\right) &= (x+\alpha y)\delta\left(n_{R_2}-1\right)+(1-\alpha)y\delta\left(n_{R_2}\right),\\ p\left(n_{R_2}\middle|n_{R_1}=0\right) &= (y+\alpha x)\delta\left(n_{R_2}\right)+(1-\alpha)x\delta\left(n_{R_2}-1\right), \end{aligned} \qquad (5)$$

where n_{R_1} is the variable associated with the central atom. Also $\alpha = \alpha_1^{AB}$ and $x + y = 1$.

The construction of the operator corresponding to the conditional probability density for the occupation variable has been discussed in detail in a previous article.[22] Here we mention only the final form of augmented space operators associated with the conditional probability density given by Eq. (4) as

$$\begin{aligned} \widetilde{N}^{(R)}_{\rm corr} = {} & x p_1^0\otimes p_R^0 + y p_1^0\otimes p_R^1 + X_1\ p_1^1\otimes p_R^0 + X_2\ p_1^1\otimes p_R^1\\ & + U_1\ p_1^0\otimes\left(\tau_R^{01}+\tau_R^{10}\right) + U_2\ p_1^1\otimes\left(\tau_R^{01}+\tau_R^{10}\right)\\ & + U_3\left(\tau_1^{01}+\tau_1^{10}\right)\otimes p_R^0 + U_4\left(\tau_1^{01}+\tau_1^{10}\right)\otimes p_R^1\\ & + U_5\left(\tau_1^{01}+\tau_1^{10}\right)\otimes\left(\tau_R^{01}+\tau_R^{10}\right), \end{aligned} \qquad (6)$$

where p_k^0 and p_k^1 denote the projection operators and τ_k^{01} and τ_k^{10} are the transfer operators. The constants are defined as

$$\begin{aligned} X_1 = x-\alpha(x-y), \quad X_2 = y+\alpha(x-y),\\ U_1 = x\sqrt{(1-\alpha)y(x+\alpha y)} + y\sqrt{(1-\alpha)x(y+\alpha x)}, \end{aligned}$$

$$U_2 = y\sqrt{(1-\alpha)y(x+\alpha y)} + x\sqrt{(1-\alpha)x(y+\alpha x)},$$
$$U_3 = \alpha\sqrt{xy}, \quad U_4 = -\alpha\sqrt{xy},$$
$$U_5 = \sqrt{xy}[\sqrt{(1-\alpha)y(x+\alpha y)} - \sqrt{(1-\alpha)x(y+\alpha x)}].$$

We should also mention at this point that the augmented space operator $\widetilde{N}^{(R)}$ associated with independent probability density $p_R(n_R)$ is

$$\widetilde{N}^{(R)} = x\ p_R^0 + y\ p_R^1 + \sqrt{xy}\left(\tau_R^{01} + \tau_R^{10}\right). \tag{7}$$

The next step is to use these operators and the central theorem for correlated random variables to set up an effective Hamiltonian in augmented space for the phonon problem. For the phonon problem, Fourier transform of the configuration averaged Green's function for a disordered binary alloy is given by

$$\bar{G}(\mathbf{k}, w^2) = \frac{1}{N}\sum_{R\ R'} e^{i\mathbf{k}\cdot(\mathbf{R}-\mathbf{R}')}\langle\langle R|(\mathbf{M}w^2 - \mathbf{D})^{-1}|R'\rangle\rangle, \tag{8}$$

where

$$\mathbf{M} = \sum_R m_R P_R,\ m_R = m^A n_R + m^B(1-n_R),$$
$$\mathbf{D} = \sum_R \Phi_{RR} P_R + \sum_{R,R'\neq R} \Phi_{RR'} T_{RR'},$$

along with the sum rule,

$$\Phi_{RR} = -\sum_{R'\neq R} \Phi_{RR'},$$

and in terms of random variables,

$$\Phi_{RR'} = \Phi_{RR'}^{AA} n_R n_{R'} + \Phi_{RR'}^{BB}(1-n_R)(1-n_{R'}) + \Phi_{RR'}^{AB}\{n_R(1-n_{R'}) + (1-n_R)n_{R'}\}. \tag{9}$$

Here R and R' refer to lattice positions. P_R is the projection operator $|R\rangle\langle R|$ and $T_{RR'}$ is the transfer operator $|R\rangle\langle R'|$ in the space spanned by the basis $\{|R\rangle\}$. $\mathbf{M}$ and $\mathbf{D}$ are the mass and dynamical matrices in vibrational mode space.

The notation on the left side of Eq. (8) requires explanation. The Fourier transform of $G(R,R',\omega^2) = \langle R|(\mathbf{M}\omega^2 - \mathbf{D})^{-1}|R'\rangle$ (for a given configuration) can only be defined *after* we configuration average and restore lattice translation symmetry. $\bar{G}(\mathbf{k},\omega^2)$ is the Fourier transform of the configuration average and *not* the average of the Fourier transform. This is explicit in the right side of Eq. (8).

A convenient way of representing states in the configuration space $\mathbf{\Psi} = \prod_R^{\otimes} \Psi_R$ is the use of the *cardinality sequence*, which is basically the sequence of sites $\{C\}$ at which one has an atom of type B corresponding to the value of random variable $n_R = 1$. In the language of the Ising model, we denote such a state by a $\downarrow$ configuration and those sites occupied by an atom of type A by $\uparrow$. For example, for the state $\{C\} = |\{\downarrow_2, \downarrow_5, \downarrow_7, \ldots\}\rangle$, the site numbers 2,5,7, ... are occupied by B atoms. If we define $|\{\uparrow, \uparrow, \ldots, \uparrow, \ldots\}\rangle$ as the *reference* configuration, then the *cardinality sequence* of this configuration is a null sequence $\{\emptyset\}$.

According to the augmented space theorem,

$$\bar{G}(\mathbf{k}, w^2) = \langle \mathbf{k}\otimes\{\emptyset\}|(\widetilde{\mathbf{M}}w^2 - \widetilde{\mathbf{D}})^{-1}|\mathbf{k}\otimes\{\emptyset\}\rangle, \tag{10}$$

where the augmented $\mathbf{k}$-space basis has the form

$$|\mathbf{k}\otimes\{\emptyset\}\rangle = \frac{1}{\sqrt{N}}\sum_R e^{-i\mathbf{k}.\mathbf{R}}|R\otimes\{\emptyset\}\rangle.$$

That configuration averaging restores lattice translation symmtery is reflected in the fact that in the subspace of augmented space spanned by the cardinality sequence $\{\emptyset\}$ we do have lattice translational symmetry. This has been discussed earlier by Mookerjee.[21]

The augmented space operators $\widetilde{\mathbf{M}}$ and $\widetilde{\mathbf{D}}$ are constructed from the original random operators [Eq. (9)] by replacing all the random variables $\{n_R\}$ associated with correlated disorder (i.e., n_R corresponding to the sites in the nearest neighbor shell of the central site) by $\widetilde{N}_{\rm corr}^R$ [given by Eq. (6)] and all the other variables $\{n_R\}$ associated with uncorrelated disorder by $\widetilde{N}^R$ [given by Eq. (7)]. $\widetilde{\mathbf{M}}$ and $\widetilde{\mathbf{D}}$ are the operators in the enlarged augmented space $\mathbf{\Xi} = \mathcal{H}\otimes\mathbf{\Psi}$, which contains the information about both the real Hilbert space and the statistical fluctuation of the system arising out of disorder.

Keeping in mind the two forms of operator $\widetilde{N}$ (i.e., $\widetilde{N}_{\rm corr}^R$ and $\widetilde{N}^R$, one indicating the signature of correlated disorder cluster with conditional probability and the other the rest of the homogeneous disordered medium), the augmented space operators $\widetilde{\mathbf{M}}$ and $\widetilde{\mathbf{D}}$ can be expressed as

$$\widetilde{\mathbf{M}} = m_B\widetilde{\mathcal{I}}\otimes I + \delta m\left[\sum_{R\notin\text{corr}}\widetilde{N}^R + \sum_{R\in\text{corr}}\widetilde{N}_{\rm corr}^R\right]\otimes P_R, \tag{11}$$

$$\widetilde{\mathbf{D}}_{\rm off} = \left[\sum_{R\notin\text{corr}}\sum_{R'\notin\text{corr}}\left\{\Phi_{RR'}^{BB}\widetilde{\mathcal{I}} + \Phi_{RR'}^{(1)}(\widetilde{N}^R + \widetilde{N}^{R'}) + \Phi_{RR'}^{(2)}\widetilde{N}^R\widetilde{N}^{R'}\right\} + \sum_{R\in1}\sum_{R'\in\text{corr}}\left\{\Phi_{RR'}^{BB}\widetilde{\mathcal{I}} + \Phi_{RR'}^{(1)}\left(\widetilde{N}^R + \widetilde{N}_{\rm corr}^{R'}\right) + \Phi_{RR'}^{(2)}\widetilde{N}^R\widetilde{N}_{\rm corr}^{R'}\right\}\right]\otimes T_{RR'},$$
$$= \left[\sum_{R\notin\text{corr}}\sum_{R'\notin\text{corr}}\Phi_{RR'}^{\rm uncorr} + \sum_{R\in1}\sum_{R'\in\text{corr}}\Phi_{RR'}^{\rm corr}\right]\otimes T_{RR'},$$
$$\widetilde{\mathbf{D}}_{\rm dia} = -\left[\sum_{R\notin\text{corr}}\sum_{R'\notin\text{corr}}\Phi_{RR'}^{\rm uncorr} + \sum_{R\in1}\sum_{R'\in\text{corr}}\Phi_{RR'}^{\rm corr}\right]\otimes P_R,$$
$$\widetilde{\mathbf{D}} = \widetilde{\mathbf{D}}_{\rm dia} + \widetilde{\mathbf{D}}_{\rm off}, \tag{12}$$

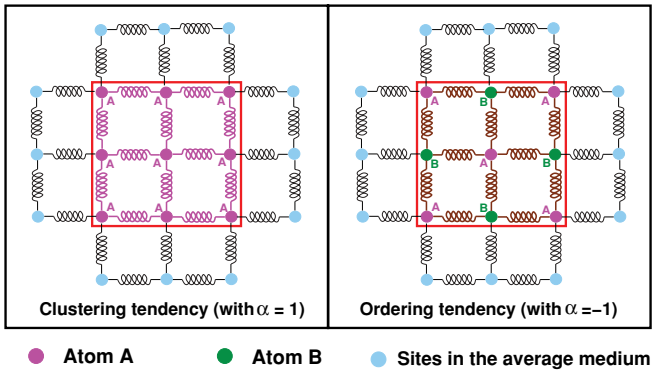

FIG. 2. (Color online) Multiple scattering picture for the disordered alloy with SRO. The left panel shows a clustering tendency while the right panel shows an ordering tendency. The range of short-range correlation is extended up to the second nearest neighbors in this cartoon diagram [shown by the red box].

where

$$\delta m = m^A - m^B, \quad \Phi^{(1)}_{RR'} = \left(\Phi^{AB}_{RR'} - \Phi^{BB}_{RR'}\right),$$
$$\Phi^{(2)}_{RR'} = \left(\Phi^{AA}_{RR'} + \Phi^{BB}_{RR'} - 2\Phi^{BB}_{RR'}\right).$$

Once the augmented space operators $\widetilde{\mathbf{M}}$ and $\widetilde{\mathbf{D}}$ are constructed, the configuration averaged Greens function is obtained from Eq. (10) using the recursion method of Haydock *et al.*[12] The recursion method in the context of the phonon problem has been described in earlier papers, and hence we refer the reader to Ref. 23 for more details.

In terms of the multiple scattering picture, the above mathematical formulation can explain a number of situations describing the short-range correlations depending on the value of the Warren–Cowley parameter α. Out of various other possibilities, the tendency of clustering and ordering are described in Fig. 2 for the two extreme values of α (+1 and −1) for a 50-50 alloy. The left panel shows the clustering tendency with the effect of short-range correlation maintained till the second nearest neighbor [shown by the red box], and the right panel shows the ordering tendency with the same range of correlation.

C. Important quantities

Once the Fourier transform of the averaged Green's function $\bar{G}(\mathbf{k},w^2)$ is calculated, the spectral function is obtained as

$$A(\mathbf{k},w^2) = -\frac{1}{\pi}\Im m\bar{G}(\mathbf{k},w^2). \tag{13}$$

A more frequently used quantity is the *coherent scattering structure factor* $S_{\rm coh}(\mathbf{k},w^2)$, which is basically the same as the spectral function except that the fluctuation in the scattering length of different atomic species is also included in the definition of $S_{\rm coh}$. All of our results are based on the structure factor. The dispersion curves for different modes are then obtained by numerically calculating the peak frequencies of these structure factors.

The disorder-induced widths are the quantities which are more sensitive to the effect of randomness as compared to dispersion, and as such are one of the focuses of the present work. In order to extract these full widths at half maxima (FWHM), we have fitted the coherent structure factors to Lorenzians exactly as experimentalists do to extract the same.

The SRO-dependent phonon DOS is obtained by integrating the structure factor over the Brillouin zone,

$$n(w,\alpha) = \sum_\lambda \langle\langle n_\lambda(w,\alpha)\rangle\rangle = -\frac{2}{3\pi}\frac{1}{\Omega_{\rm BZ}}\sum_\lambda \int_{\rm BZ} \Im m[\bar{G}_\lambda(\mathbf{k},w^2)]wdw \tag{14}$$

where λ is the normal-mode branch index and α is the SRO parameter. The normal modes are tracked from the complex band structures obtained from the configuration averaged Green's functions.

The lattice heat capacity (C_v^β) of a phase (β) is determined by its phonon DOS $n(w,\alpha)$. The difference $\Delta C_v^{\beta-\beta'}$ for two phases β and β' of a compound depends on the difference in their phonon DOS as

$$\Delta C_v^{\beta-\beta'}(T,\alpha) = 3Nk_B\int_0^\infty [n^\beta(w,\alpha) - n^{\beta'}(w,\alpha)] \times \left(\frac{h\nu}{k_BT}\right)^2 \frac{e^{h\nu/k_BT}}{(e^{h\nu/k_BT}-1)^2}d\nu, \tag{15}$$

where $w = 2\pi\nu$.

The thermodynamic importance of vibrational entropy has often been neglected, but recent measurements show that it affects the relative stability of chemically ordered and disordered phases.[6,20,24] As a matter of fact, in many systems, the vibrational entropy difference between two phases comes out to be comparable to the configurational entropy difference. The difference in vibrational entropy of two phases β and β', $\Delta S_{\rm vib}^{\beta-\beta'}$, can be obtained from the difference in their lattice heat capacity $\Delta C_v^{\beta-\beta'}$ as

$$\Delta S_{\rm vib}^{\beta-\beta'}(T,\alpha) = \int_0^T \frac{\Delta C_v^{\beta-\beta'}(T',\alpha)}{T'}dT'. \tag{16}$$

In the higher temperature limit ($T \geqslant \Theta_{\rm Debye}$), the combination of Eqs. (15) and (16) yields

$$\Delta S_{\rm vib}^{\beta-\beta'}(\alpha) = -3Nk_B\int_0^\infty [n^\beta(\nu,\alpha) - n^{\beta'}(\nu,\alpha)]\ln(\nu)\,d\nu. \tag{17}$$

Configurational entropy is a measure of the degree of disorder for an alloy. For a homogeneously disordered binary alloy, the configurational entropy is given by

$$S_{\rm homog} = -k_B[x\ln(x) + (1-x)\ln(1-x)]. \tag{18}$$

This approximation assumes that all the lattice sites are equivalent and uncorrelated. However in an alloy with a certain degree of order, not all lattice sites are equivalent and a certain degree of correlation always exists between lattice positions. In the case of SRO, there exists a finite cluster up to which the correlation between sites remains stronger and decays rapidly with increasing distance. All the correlations are described within the basic cluster and the rest of the lattice sites are considered to be homogeneously disordered. Since one of our focuses in this article is to describe states with a certain degree of SRO, we choose the basic clusters to be pairs for simplicity.

The configurational entropy (including pairs up to the nth nearest neighbor distance) for a random binary alloy with SRO is given by

$$S_{\rm corr}^{(n)} = S_{\rm homog} - S_{\rm homog}\left(\sum_{j=1}^{n} N^{(j)}\right) - k_B \sum_{j=1}^{n} \frac{N^{(j)}}{2} \times \left[P_j^{AA} \ln\left(P_j^{AA}\right) + 2P_j^{AB} \ln\left(P_j^{AB}\right) + P_j^{BB} \ln\left(P_j^{BB}\right)\right], \quad (19)$$

where $N^{(j)}$ denotes the number of atoms in the jth neighboring shell, Also the pair probabilities P_j's are given by

$$P_j^{AA} = y^2 + xy\alpha_j, \quad P_j^{AB} = xy(1-\alpha_j), \quad P_j^{BB} = x^2 + xy\alpha_j,$$

where α_j is the SRO parameter in the jth nearest neighbor shell.

It is easy to verify that for $\alpha_j = 0(\forall j)$, $S_{\rm corr}$ reduces to $S_{\rm homog}$. In addition, the terms under the summations converge to zero with increasing distance, meaning that lattice sites separated by large distances are uncorrelated. In our case of a bcc disordered alloy, we verified that the inclusion of third neighbor pairs modifies the entropy only by 0.005%, confirming the short-range nature of the correlations.

III. COMPUTATIONAL DETAILS

The *Ab initio* Quantum-ESPRESSO code[25] has been used to compute the Fe-Fe, Fe-Cr, and Cr-Cr dynamical matrices at different bond lengths with different ordered structures. Force constants for B2 Fe-Cr, DO_3 Fe_3Cr and $FeCr_3$, and bcc Fe and bcc Cr at their equilibrium lattice parameters have been used to estimate the random alloy dynamical matrix. Quantum-ESPRESSO is based upon the density functional perturbation theory (DFPT),[26] which is basically a linear response method to study the electronic structure and phonon excitations in condensed matter systems. Within this method, the dynamical matrix associated with the lattice dynamics of the system can be obtained from the ground state electron charge density and its linear response to a distortion of the nuclear geometry. In terms of computational efficiency, one of the greatest advantages of the DFPT (as compared to other nonperturbative methods) is that within this method the responses to perturbation of different wavelengths are decoupled. This feature allows one to calculate phonon frequencies at arbitrary wave-vectors avoiding the use of super cells and with a workload that is independent of the phonon wavelength. The calculations were done at the alloy lattice constants: $a = 2.873$ Å for $Fe_{75}Cr_{25}$, $a = 2.876$ Å for $Fe_{50}Cr_{50}$, and $a = 2.879$ Å for $Fe_{25}Cr_{75}$. Ultrasoft pseudopotentials with nonlinear core corrections[27] were used. PBE-96 spin-polarized generalized gradient approximate (GGA) functionals were used for the exchange-correlation part of the potential. The reason for choosing GGA functionals is its better capability to calculate the ground state properties. Plane waves with energies of up to 55 Ry are used in order to describe electron wave function, and Fourier components of the augmented charge density with cutoff energies of up to 650 Ry are taken into account. The Brillouin zone integrations are carried out with Methfessel-Paxton smearing[28] using a $14 \times 14 \times 14$ **k**-point mesh. The value of the smearing parameter is 0.01 Ry. These parameters are found to yield phonon frequencies converged to within 5%. Once the electronic structure calculation is converged within a desired accuracy, the force constants are then computed first in reciprocal space on a finite **q**-point grid and then a Fourier transformation is employed to obtain the real space force constant. In this work, we have used a $8 \times 8 \times 8$ **q**-point mesh, which provides a sufficiently dense grid.

TABLE I. Dynamical matrix elements in newtons/meter obtained from Quantum-ESPRESSO codes.

Neighbors	$x = 0.0$	$x = 0.25$	$x = 0.5$	$x = 0.75$	$x = 1.0$
$111xx$	16.660	14.081	13.259	12.120	13.491
$111xy$	14.910	14.100	13.610	12.490	6.469
$200xx$	14.580	18.782	20.192	20.910	35.960
$200xy$	0.550	−1.112	−0.911	−0.165	−1.556

The masses of Fe and Cr are 55.845 and 51.996 amu, respectively, and their scattering lengths are 9.45 and 3.64 fm, respectively. For dynamical matrices of a 50-50 alloy, we have performed two sets of calculations. First is the calculations on a Fe-Cr B2 structure with Cr at the origin and Fe at the body-center which give the first nearest neighbor $\Phi_1^{\rm CrFe}$ and the second nearest neighbor $\Phi_2^{\rm CrCr}$. Next is a similar calculation but with Fe at the origin and Cr at the body-center which yields the first nearest neighbor $\Phi_1^{\rm FeCr}$ and second nearest neighbor $\Phi_2^{\rm FeFe}$. The second nearest neighbor $\Phi_2^{\rm FeCr}$ is estimated from $(\Phi_2^{\rm FeFe} + \Phi_2^{\rm CrCr})/2$.

The dynamical matrices for the compositions $Fe_{0.25}Cr_{0.75}$ and $Fe_{0.75}Cr_{0.25}$ cannot be so obtained from an ordered structure. For these compositions the dynamical matrices are estimated from the transferable force constant model proposed by van de Walle and Ceder.[18,29] The idea behind this model is to use bond-length-dependent transferable force constants. Calculations using this model on a number of systems had revealed that a major part of the variation of stiffness can be explained by changes in bond length alone. This suggests that force constant vs bond length relationships exhibit better transferability than the force constants themselves. Table I shows our estimates of the dynamical matrices.

The ASR calculation for the random alloy is done by generating a map from a real space cluster of 700 atoms. The disorder in the force constants was considered till the second nearest neighbor shell, which consists of 14 sites for a bcc structure. The phonon DOS is calculated on a frequency mesh of 1001 points with a small smearing of 0.005. However for a more accurate calculation of vibrational entropy, the phonon DOS used in the entropy expression was calculated at 2001 points.

In terms of computational efficiency, one of the advantages of **k**-space recursion (over the real space one) is the possibility of working in an enormously reduced space (compared to the Hilbert space required in the real space recursion method). It can be shown explicitly[30] that the operation of an effective Hamiltonian (in the **k**-space recursion method) can entirely be done in configuration space only and the calculation does not require us to involve the Hilbert space $\mathcal{H}$ at all. Thus, for example, for a system with N sites and m possible

realizations of the random variables associated with each site, the augmented space involved $N \times m^N$ basis functions. The standard real space method for implementing this on a computer would require handling impossibly large $(Nm^N) \times (Nm^N)$ matrices. The first reduction of computational cost in a **k**-space recursion comes in the form of dealing with smaller subspaces of such a huge product space. Since in the **k**-space recursion one is required to deal only with the configuration space, instead of handling the enormously large matrix of rank $(Nm^N) \times (Nm^N)$, one needs to work with a matrix of rank $(m^N) \times (m^N)$ only. In addition, the approximation involved in truncating the full lattice to a large cluster (in real space method) is also avoided. Second, we can utilize the local symmetries of the configuration space (as described earlier[31]) to further reduce its rank. Finally we have used memory reduction and time saving for ASR by taking advantage of multispin coding techniques. In other words, one can utilize the bit manipulation technique and predefined logical functions in the computer to store the basis vectors of configuration space in bits associated with different words.

IV. RESULTS AND DISCUSSION

In the first part of this section, we initially focus on the lattice dynamics of three bcc $Fe_{1-x}Cr_x$ ($x = 0.25$, 0.47, and 0.75) alloys. The present study is based on the phonon dispersion, phonon DOS, lattice heat capacity, and vibrational and configurational entropy for these alloys. The trend and the magnitude of the phonon entropy as a function of the alloy composition (x) is discussed in some detail. We also provide a plausible explanation for our smaller value of vibrational entropy of mixing (compared to other findings). Our next focus is to investigate the effect of the local chemical environment on the vibrational properties of the bcc $Fe_{50}Cr_{50}$ alloy. The effect of local environment will be studied via the Warren–Cowley SRO parameter.

A. $Fe_{1-x}Cr_x$ alloy ($x = 0.25, 0.47, 0.75$)

In Fig. 3 we display the phonon dispersion curves for the three $Fe_{1-x}Cr_x$ ($x = 0.25$, 0.47, and 0.75) alloys. The error bars in all the three panels represent the FWHM at various ζ values. Interestingly, the gross feature of dispersion for all the three alloys, including the Cr-rich $Fe_{25}Cr_{75}$, resemble much more the phonon dispersion of bcc Fe than that of bcc Cr. The disorder-induced linewidths on the other hand vary from one alloy to another along the different high symmetry directions. The Cr-rich alloy tends to have a larger width (i.e., smaller phonon lifetime) than the other two alloys. Being dominated by the force constant disorder, we expect ASR to perform a good job (as done before[17] as well in the case of the NiPt alloy) in capturing the essential off-diagonal disorder in the present case. The advantage of ASR over the other approximate theories (VCA or single-site CPA) is more significant if one looks at the feature of phonon dispersion at higher wave-vectors, where the improper inclusion of the disorder effect in other theories deviates the dispersion curves lower in frequency and away from the one calculated from ASR (as well as those measured). The distinction in the low wave-vector regime is not that big, because the self-averaging

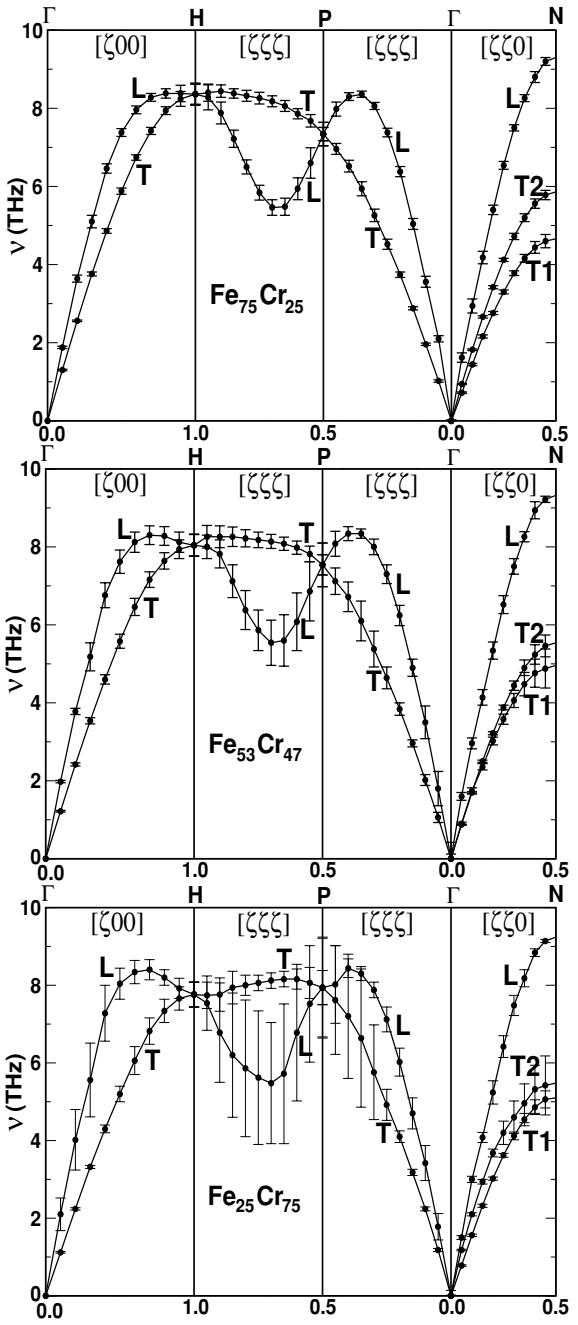

FIG. 3. Phonon dispersion curves for three $Fe_{1-x}Cr_x$ ($x = 0.25$, 0.47, and 0.75) alloys. The error bar in all three panels represent the FWHM at various ζ values.

of both masses and force constants over a single wavelength reduces the result of ASR or any other accurate theory to become close to VCA.

The phonon DOS for the three alloys along with those of pure bcc Fe and bcc Cr are shown in Fig. 4. As reflected by the dispersion curves, the phonon DOS for all three alloys resembles much more the phonon DOS of bcc Fe than that of bcc Cr. The overall shape of the phonon DOS curves calculated in the present work is similar to the previous findings[5,6] for an almost similar alloy composition. Since the change in the phonon DOS as Cr is added to bcc Fe is rather

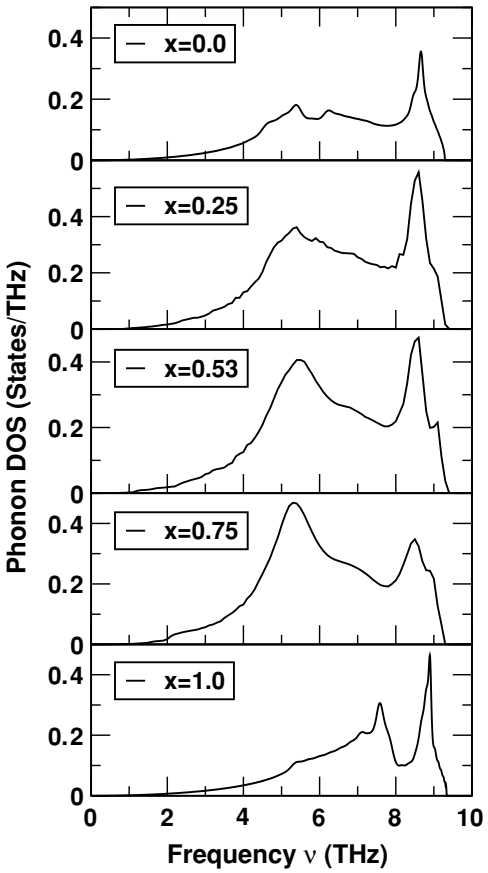

FIG. 4. Phonon DOS for pure bcc Fe, bcc Cr, and the three $Fe_{1-x}Cr_x$ ($x = 0.25$, 0.47, and 0.75) alloys.

small, there should in fact be little difference in the integral $\int_0^\infty n(\nu)\ln(\nu)\,d\nu$ for bcc Fe and that of the three alloys. This will be shown more explicitly by our data on the vibrational entropy for these sets of alloys.

The temperature dependence of the vibrational entropy of mixing for the three $Fe_{1-x}Cr_x$ alloys is shown in Fig. 5. This entropy difference is calculated by using Eq. (16), where $S_{\rm vib}(x)$ (β state) is the vibrational entropy of the alloy with composition x, and $S_{\rm vib}^{\rm avg}(\beta'$ state) is the average of the chemically unmixed state of bcc Fe and bcc Cr weighted by the factors 75 : 25, 53 : 47, and 25 : 75 for the alloys $Fe_{75}Cr_{25}$, $Fe_{53}Cr_{47}$, and $Fe_{25}Cr_{75}$, respectively. The inset shows a similar estimate of the difference in lattice heat capacity between each of the bcc Fe-Cr alloys and the corresponding chemically unmixed state. It is immediately clear from the inset that the specific heat curves have similar shapes, but increase in weight with the concentration of Cr. Because of the similar shape of the phonon DOS curve of the alloy and that of the DOS curve for pure Fe, a linear scaling of $\Delta C_{\rm v}(T)$ with the Cr concentration x is expected. Our theoretical as well as experimental estimates of vibrational entropies are shown in Table II. Notice our calculated values are smaller than those obtained experimentally.[5,20]

How can we explain the apparent discrepancy between our findings (smaller entropy difference) and the results from inelastic neutron scattering?[5,20] One of the reasons for such a discrepancy is the so-called neutron weighting problem[20] in

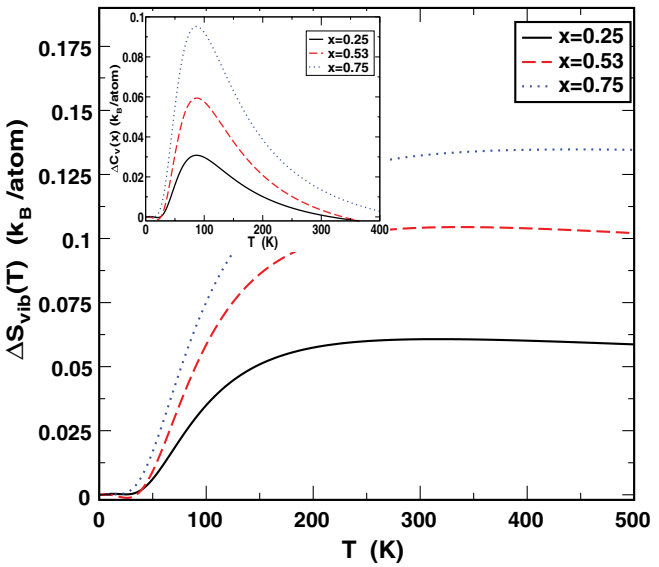

FIG. 5. (Color online) Temperature dependence of phonon entropy of mixing $\Delta S_{\rm vib} = S_{\rm vib}(x) - [xS_{\rm vib}^{\rm Cr} + (1-x)S_{\rm vib}^{\rm Fe}]$ for the three $Fe_{1-x}Cr_x$ alloys. The inset shows a similar estimate of the difference in lattice heat capacity $\Delta C_{\rm v}(x)$ between the alloy with composition x and the corresponding chemically unmixed state.

the calculation of phonon DOS in inelastic neutron scattering measurements. For alloys, different alloy components have different efficiencies for phonon scattering, which are proportional to the ratio of their neutron scattering cross sections $\sigma_{\rm sc}$ to their atomic mass. The displacements of different atoms in different phonons usually have different amplitudes, so different phonons may be over- or underrepresented in a DOS directly obtained from experimental measurements. This distortion of phonon DOS should be corrected to get a reliable estimate of vibrational entropy. In fact for the Fe-Cr alloy, the phonon scattering from natural Fe is approximately three times stronger than that from natural Cr, i.e., $\sigma_{\rm sc}^{\rm Fe}/m_{\rm Fe} \simeq 3\,\sigma_{\rm sc}^{\rm Cr}/m_{\rm Cr}$. Such a neutron weighting problem has been investigated recently[20] for the Fe-Cr alloy, and an attempt has been made to avoid such a problem by estimating a neutron-weight-corrected phonon DOS. As a matter of fact, phonon entropy of mixing calculated from the neutron-weight-corrected DOS is

TABLE II. Theoretical and experimental vibrational entropies. x is the concentration of Cr.

Theoretical $\Delta S_{\rm vib}(x)$			
x	$T = 150$ K	$T = 300$ K	$T = \infty$
0.25	0.051	0.063	0.0615
0.53	0.085	0.104	0.0999
0.75	0.107	0.132	0.1155
Experimental $\Delta S_{\rm vib}(x)$[5,20] at similar x			
x	$T = 150$ K	$T = 300$ K	$T = \infty$
0.30	0.098	0.128	0.141
0.53	0.142	0.184	0.201
0.70	0.148	0.194	0.214

smaller than that evaluated from the directly measured DOS. This is an indication of the right trend of our calculated phonon entropy of mixing if the measured phonon DOS accurately takes into account the effect of different efficiencies of phonon scattering for alloy components. A related reason for the mentioned discrepancy can be attributed to the use of the VCA for analyzing the coherent inelastic neutron scattering data from chemically disordered alloys. The VCA does not allow for high frequency vibrations in disordered alloys at the frequencies of optical modes in the ordered alloys. It, therefore, may overestimate the change in phonon DOS upon chemical ordering. In addition, it has also been mentioned by Fultz *et al.*[5] that the absolute error in the value of vibrational entropy of mixing ($\Delta S_{\rm vib}$) obtained from their inelastic neutron scattering experiment can be as large as $0.05\,k_B$/atom. Keeping this error in mind, our theoretical phonon entropy of mixing then is in the same ballpark as that measured by them.

In order to understand the general trend of the phonon entropy of mixing with varying alloys, we shall next make a connection with a more intrinsic quantity, the so-called FWHM associated with the disorder-induced lifetime broadening of the phonon groups. Lifetime broadening is a consequence of the local vibrational modes mainly arising out of the disorder in the interatomic force constants. Figure 6 shows the FWHM as a function of the wave-vector magnitude ($|\zeta|$) along the high-symmetry directions for the three bcc $Fe_{1-x}Cr_x$ alloys. One can easily notice that the disorder broadening increases quite rapidly as we move toward the Cr-rich alloy. For example, the maximum value of linewidth along the H-P direction for the $Fe_{75}Cr_{25}$ alloy is $\simeq$0.4 THz, however it increases to $\simeq$0.78 THz for the $Fe_{53}Cr_{47}$ alloy and increases further to $\simeq$1.85 THz in case of the $Fe_{25}Cr_{75}$ alloy. A damped harmonic oscillator function fit to the two phonon groups (one along [100] and the other along [111]) for the $Fe_{53}Cr_{47}$ alloy has been made by Fultz *et al.*[5] They estimated a resonance width of 0.2 THz for the [100] $Q = 0.5$ phonon group and 0.96 THz for the [111] $Q = 0.6$ phonon group. We obtained a similar estimate for the widths for the $Fe_{53}Cr_{47}$ alloy. Broadened peaks were also observed for phonons near Brillouin zone boundaries.

Usually the line broadening of the phonon groups is more if the strength of the disorder is more, which causes smearing of the sharp features in the phonon DOS curves for the alloys. Such a smoothening of the vibrational energy spectrum will have benign consequences on the phonon entropy calculation provided the phonon structure factors are broadened neither too asymmetrically nor excessively toward low frequencies. The phonon line shapes in our calculations for $Fe_{75}Cr_{25}$ and $Fe_{53}Cr_{47}$ came out to be quite symmetric except in some of the higher frequency regimes. The line shapes for the Cr-rich $Fe_{75}Cr_{25}$ alloy are comparatively less symmetric with a larger disorder broadening. Keeping in mind the magnitude of the calculated vibrational entropy difference for the three alloys as quoted before and looking at the FWHM for the same three alloys in Fig. 6, one can arrive at a conclusion that the disorder broadening of the phonon groups tends to increase the phonon entropy of mixing. Such a theoretical prediction has also been supported by previous experimental investigations.[5]

In Fig. 7, we display the phonon entropy of mixing as a function of alloy composition (x) at different temperatures (T). The high-temperature limits of $\Delta S_{\rm vib}$ were obtained from

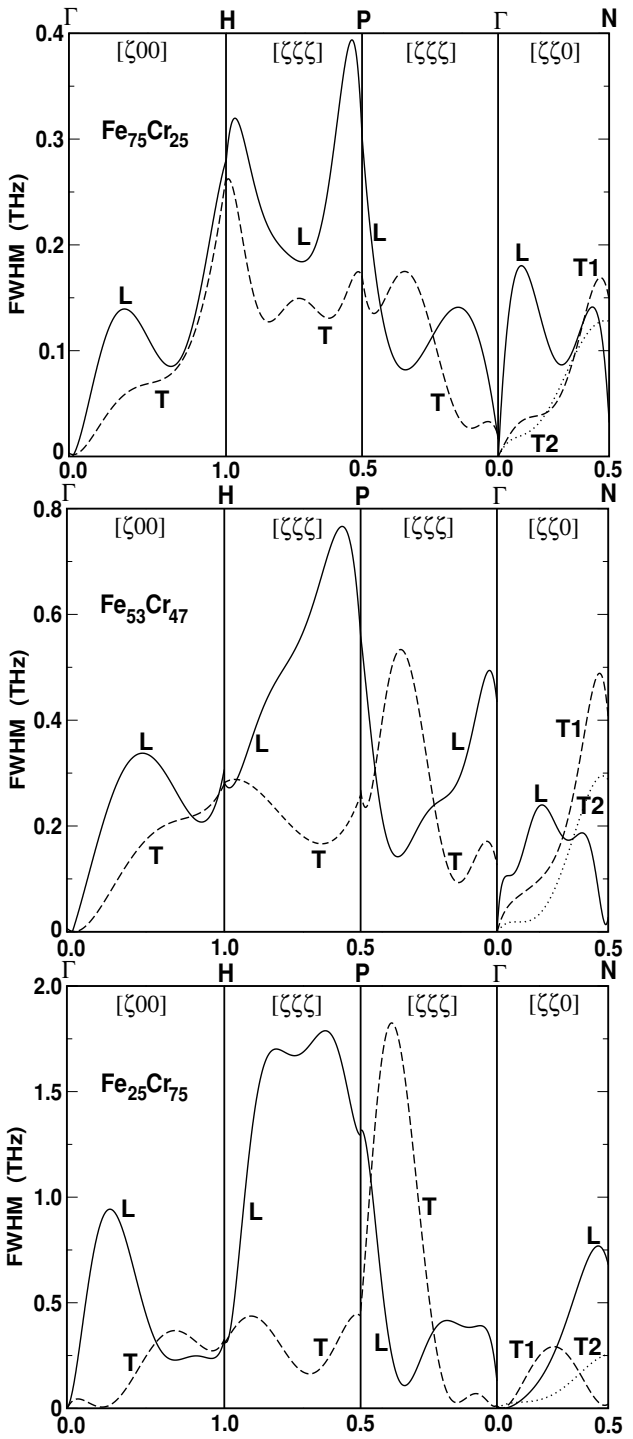

FIG. 6. Disorder-induced FWHM along the high-symmetry directions for three $Fe_{1-x}Cr_x$ ($x = 0.25$, 0.47, and 0.75) alloys.

Eq. (17) and are shown in Fig. 7 by the blue-dotted curve. The configurational entropy of the fully random solid solution is also plotted to show the relative magnitude of the phonon entropy.

It is expected intuitively that all thermodynamic functions should change monotonically during spinodal decomposition. A smooth change occurs for configurational entropy for example. However, due to the small changes in the phonon DOS curve, the phonon entropy will not change significantly

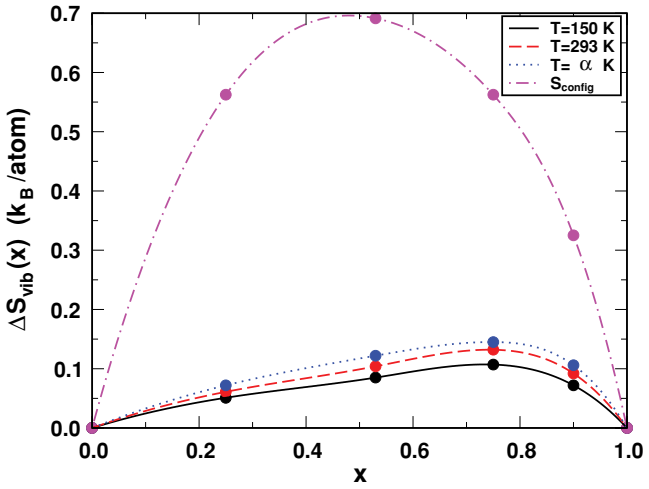

FIG. 7. (Color online) Concentration dependence of phonon entropy of mixing $\Delta S_{\rm vib}(x)$ at various fixed temperatures. The high-temperature ($T \to \infty$) limit of $\Delta S_{\rm vib}(x)$ is calculated from Eq. (17). The composition dependence of the configurational entropy (indicated by the magenta dot-dashed line) for the fully random solid solution is also shown to compare the relative magnitude of the phonon entropy of mixing.

during the early stages of spinodal decomposition. For the Fe-Cr alloy, the transition of the shape of the phonon DOS curve from being Fe-like to Cr-like occurs at high Cr concentration. Therefore, vibrational entropy affects differently the solubility of Fe in a bcc Cr-rich phase compared to the solubility of Cr in a bcc Fe-rich phase. Although this asymmetry does not occur for the configurational entropy of mixing, the phonon entropy has a different dependence on composition (x) and hence the reason for an asymmetric curve in Fig. 7. This is precisely the reason that the inclusion of vibrational entropy into the alloy thermodynamics alters the shapes of phase boundaries and does not simply rescale the temperature of the miscibility gap. The critical temperature and composition of the miscibility gap in Fe-Cr are 905 K and $x = 0.51$, respectively.[32] As a matter of fact, it has been found that, in the absence of phonon entropy of mixing, the miscibility gap shifts up in temperature and toward pure Cr, with a critical temperature and composition of 1208 K and $x = 0.64$, respectively. Thus the role of phonon entropy is to lower the critical temperature of the miscibility gap and shift it toward the equiatomic composition.

B. Short-range ordering effect

The existence of intermetallic phases in compounds is a consequence of the strong ordering tendency of the alloy. The same driving forces, in various systems, make the alloy exhibit chemical SRO in that phase. Depending on the system of interest, the chemical SRO might result in a complete ordering or a phase segregating tendency or even in a combination of the two. Although a few experimental works[7,33] which study the effects of the local chemical environment on the lattice dynamics of disordered alloys exist, a reliable theoretical understanding of the same from a first-principles calculation is still lacking. The present investigation is undertaken to analyze the effects of the local atomic environment (via the Warren–Cowley SRO parameter α) on three basic lattice dynamical properties, namely, phonon DOS and vibrational and configurational entropies within a first-principles calculation.

For Fe-Cr alloys, Bonny *et al.*[9] and Erhart *et al.*[10] have shown using atomistic simulations that there is the possibility of SRO in these alloys. References 5–8 of Erhart *et al.*[10] report experimental work on Fe-Cr whose data can be explained by assuming the existence of SRO in Fe-Cr alloys.

Figure 8 shows how the phonon density of states for a 50-50 Fe-Cr alloy changes as a function of the Warren–Cowley short-range order parameter (α). The two extreme limits $\alpha = -1$ and $+1$ correspond to the tendency toward ordering and phase segregation, respectively. The DOS for the completely random (homogeneously disordered) alloy ($\alpha = 0$) is also shown for the sake of comparison. It is clear from the figure that the alloys show moderate differences in DOS for samples with chemical SRO. A general connection between the phonon DOS and chemical SRO may be made from the slopes of the phonon dispersion curves. A high density of phonon states is obtained from flat dispersion curves,

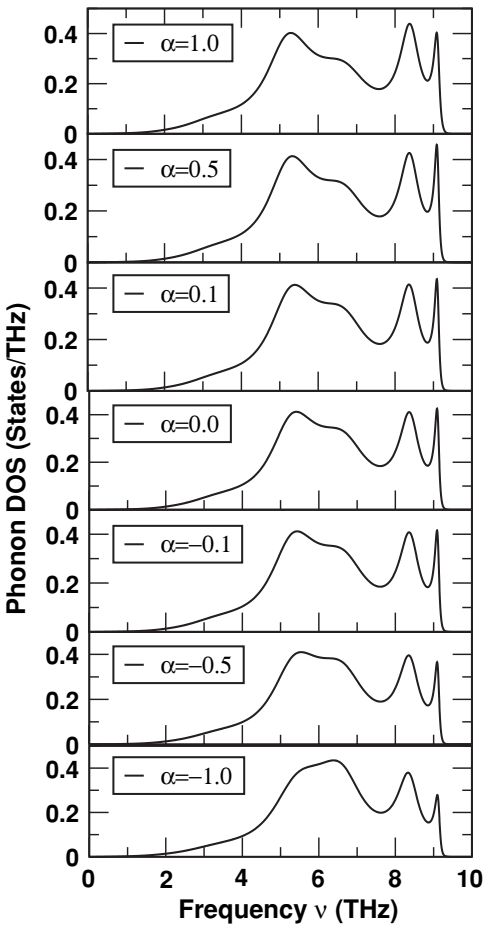

FIG. 8. Local chemical environmental effect on the phonon DOS of the $Fe_{50}Cr_{50}$ alloy. The phonon DOS of fully random solid solution ($\alpha = 0$) is also plotted for the sake of comparison. The local environmental effect is dictated via the Warren–Cowley SRO parameter (α). $\alpha = -1$ indicates an ordering tendency, $\alpha = +1$ indicates a clustering (phase segregating) tendency, and $\alpha = 0$ corresponds to a fully random solid solution with no SRO.

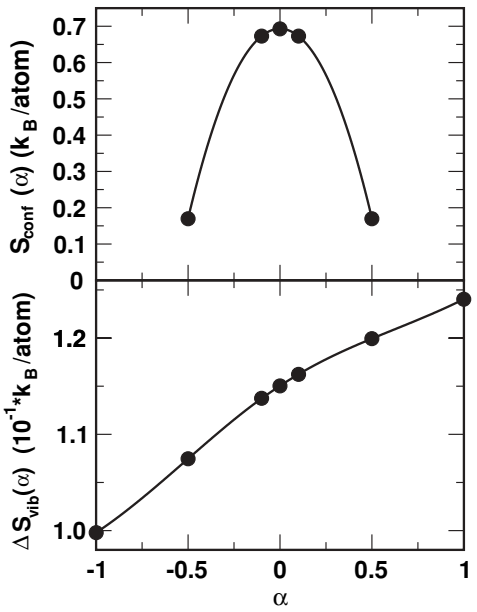

FIG. 9. SRO dependence of the configurational and phonon entropy of mixing for a disordered $Fe_{50}Cr_{50}$ alloy.

especially when they include Brillouin zone boundaries. They also provide a slow group velocity of sound. Much of the energy of lattice vibrations is associated with localized atomic movements for slowly propagating phonon wave packets. The SRO affects these localized atomic movements quite strongly and hence has a major effect on the corresponding regime of the phonon DOS. Those parts of the phonons DOS not associated with the flattened dispersion curves should be less sensitive to SRO. Based on these arguments, one can easily notice from Fig. 8 that the phonon DOS in the frequency range $\simeq$4.5–7 THz are mainly arising from the contribution of flat parts of the dispersion curves and hence are influenced by SRO more strongly than the feature of the DOS beyond $\simeq$7 THz.

It is even more interesting to look at the effects of SRO on the entropy of mixing. In the lower panel of Fig. 9, we display how the vibrational entropy of mixing in the high-temperature limit ($T \geqslant \Theta_{\text{Debye}}$) varies with the SRO parameter (α) for a 50-50 Fe-Cr alloy. For comparison sake, we also plotted the SRO variation of the configurational entropy (upper panel) as calculated from Eq. (19) (including only the first nearest neighbor shell SRO effect $\alpha = \alpha_1$). The small variation of phonon DOS curve as a function of SRO parameter is also reflected in the phonon entropy of mixing. For the homogeneously disordered ($\alpha = 0$) $Fe_{50}Cr_{50}$ alloy, the phonon entropy of mixing came out to be 0.115 k_B/atom. However, in different local chemical environments, the phonon entropy of mixing ranges from 0.099 k_B/atom (for $\alpha = -1$) to 0.124 k_B/atom (for $\alpha = +1$), which is not a big change compared to the completely random solid solution. The dependence of phonon entropy of mixing on the local arrangement of atoms delivers a deeper insight into the understanding of thermodynamic stability of complex alloys.

As obvious from the phonon DOS curves (see Fig. 4) for the three $Fe_{1-x}Cr_x$ alloys, the total DOS looks very similar to that of bcc Fe than that of bcc Cr. Unfortunately, we do not exactly know the concentration above 75 at. % of Cr for which the phonon DOS changes from being Fe-like to being Cr-like. However at low concentrations of Fe in a Cr host, there is a substantial distortion of the Fe partial DOS (PDOS) curves compared to those of pure bcc Fe. The PDOS of both Fe and Cr atoms undergo an average softening upon alloying, which leads to a net positive phonon entropy of mixing, but with a net softening of Cr PDOS to be larger than that of Fe. At low concentrations of Fe in Cr, this larger softening of Cr PDOS curves causes the phonon entropy of mixing to increase rapidly with Fe concentration, yielding a skewed shape of the concentration dependence of phonon entropy (see Fig. 7). The interplay of such softening of phonon modes in alloys with SRO is even more dramatic, because in this case the total phonon entropy of mixing is not just affected by the different entropic weights of their atomic species, but also by the nature of correlated disorder present in the short-range clusters considered.

The main reason behind investigating the SRO dependence of the phonon DOS and phonon entropy in the present work was to satisfy ourselves and at the same time provide a validation for our correct smaller value of phonon entropy of mixing compared to other findings. It was our intuition that the SRO effect might enhance the magnitude of phonon entropy of mixing to bring it closer to other findings, but we figured out that that is not the case, at least in the case of the Fe_{1-x} Cr_x alloy. And the reason we gave in Sec. IV A for the comparatively smaller value of our calculated phonon entropy is indeed valid. While this result does not restrict the possibility that SRO plays an important role in the lattice dynamics of alloys in other systems, it does indicate that the local environmental effects in Fe-Cr alloys may not be that significant.

V. CONCLUSION

We propose a combination of the first-principles Quantum-ESPRESSO method (based on the density functional perturbation theory) and the ASR method to investigate the lattice dynamics and the vibrational and configurational entropy of disordered alloys at any arbitrary concentration. A generalized formalism (within the ASR method) to include the effects of SRO on the lattice dynamics has been derived and implemented on a bcc $Fe_{1-x}Cr_x$ alloy. We studied three alloys $Fe_{25}Cr_{75}$, $Fe_{53}Cr_{47}$, and $Fe_{75}Cr_{25}$, the phonon dispersion and phonon DOS of which were much more similar to those of pure bcc Fe than those of Cr. We obtained a comparatively smaller value of phonon entropy of mixing (ΔS_{vib}) in contrast to the interpretations from previous experiments. However, in light of our results, the upper bounds of ΔS_{vib} obtained from inelastic neutron scattering data should be reinterpreted. The upper bound from the experiment is unlikely to be appropriate (i) due to the use of the VCA in analyzing their data and (ii) due to the incorrect neutron weighting caused by the difference in phonon scattering efficiencies of the two elements. A connection with the lifetime broadening of the phonon groups has been made to explain the trend of the magnitude of calculated ΔS_{vib}. A comparatively larger softening of the Cr partial DOS (compared to Fe) curves is found to be the reason behind the compositional asymmetry of the phonon entropy of mixing.

The phonon entropy shifts both the miscibility gap toward the equiatomic composition and lowers the critical temperature by ~300 K. The effect of SRO did not come out to be significant in terms of the magnitude of phonon entropy of mixing, which we initially thought not to be the case.

Understanding the magnitude of the phonon entropy variations between different states of a compound remains a central problem in any first-principles alloy theory. The effect of local arrangement of atoms on the phonon entropy provides an even higher level of detail which we studied in the present work for the Fe-Cr alloy. Although this effect turned out to be small in the Fe-Cr alloy, it still remains of interest to evaluate the magnitude of this effect in other systems.

ACKNOWLEDGMENTS

One of the authors, A.A., acknowledge financial support from the Department of Energy (DEFG 02-03ER46026). The authors thank S. Ghosh for helping run the Quantum-ESPRESSO calculation.

[1] R. J. Elliot, J. A. Krumhansl, and P. L. Leath, Rev. Mod. Phys. **46**, 465 (1974).

[2] J. K. Okamoto *et al.*, in *Microbeam Analysis-1990*, edited by J. R. Michael and P. Ingram (San Francisco Press, San Francisco, 1990), p. 56.

[3] L. Anthony, J. K. Okamoto, and B. Fultz, Phys. Rev. Lett. **70**, 1128 (1993); G. D. Garbulsky and G. Ceder, Phys. Rev. B **49**, 6327 (1994); **53**, 8993 (1996).

[4] J. L. Nagel, B. Fultz, and J. L. Robertson, Philos. Mag. B **75**, 681 (1997).

[5] B. Fultz, L. Anthony, J. L. Robertson, R. M. Nicklow, S. Spooner, and M. Mostoller, Phys. Rev. B **52**, 3280 (1995).

[6] S. M. Dubiel, J. Cieslak, W. Sturhahn, M. Sternik, P. Piekarz, S. Stankov, and K. Parlinski, Phys. Rev. Lett. **104**, 155503 (2010); W. Sturhahn, T. S. Toellner, E. E. Alp, X. Zhang, M. Ando, Y. Yoda, S. Kikuta, M. Seto, C. W. Kimball, and B. Dabrowski, *ibid.* **74**, 3832 (1995).

[7] B. Fultz, T. A. Stephens, W. Sturhahn, T. S. Toellner, and E. E. Alp, Phys. Rev. Lett. **80**, 3304 (1998).

[8] M. Goda, J. Phys. C: Solid State Phys. **6**, 3047 (1973); J. Phys. F: Metal Phys. **7**, 1421 (1977).

[9] G. Bonny, P. Erhart, A. Caro, R. C. Pasianot, L. Malerba, and M. Caro, Model Simul. Mater. Sci. Eng. **17**, 025006 (2009).

[10] P. Erhart, A. Caro, M. Serranode Caro, and B. Sadigh, Phys. Rev. B **77**, 134206 (2008).

[11] A. Mookerjee, J. Phys. C: Solid State Phys. **6**, L205 (1973).

[12] R. Haydock, V. Heine, and M. J. Kelly, J. Phys. C: Solid State Phys. **5**, 2845 (1972).

[13] D. W. Taylor, Phys. Rev. **156**, 1017 (1967).

[14] A. Gonis and J. W. Garland, Phys. Rev. B **18**, 3999 (1978); T. Kaplan, P. L. Leath, L. J. Gray, and H. W. Diehl, *ibid.* **21**, 4230 (1980).

[15] D. A. Rowlands, J. B. Staunton, B. L. Györffy, E. Bruno, and B. Ginatempo, Phys. Rev. B **72**, 045101 (2005); D. A. Biava, S. Ghosh, D. D. Johnson, W. A. Shelton, and A. V. Smirnov, *ibid.* **72**, 113105 (2005).

[16] M. K. Miller, Surf. Sci. **246**, 434 (1991); A. Cerezo, J. M. Hyde, M. K. Miller, S. C. Petts, R. P. Setna, and G. D. W. Smith, Philos. Trans. R. Soc. London Ser. A **341**, 313 (1992).

[17] A. Alam and A. Mookerjee, Phys. Rev. B **69**, 024205 (2004).

[18] A. van de Walle and G. Ceder, Phys. Rev. B **61**, 5972 (2000).

[19] G. J. Ackland, *Alloy Modelling and Designs*, edited by G. Stocks and P. Turchi (The Minerals, Metals and Materials Society, Pittsburgh, PA, 1994), p. 149.

[20] M. S. Lucas, M. Kresch, R. Stevens, and B. Fultz, Phys. Rev. B **77**, 184303 (2008).

[21] A. Mookerjee, in *Electronic Structure of Alloys, Surfaces and Clusters*, edited by D. D. Sarma and A. Mookerjee (Taylor & Francis, London, 2003).

[22] A. Alam and A. Mookerjee, J. Phys.: Condens. Matter **21**, 195503 (2009); T. Saha, I. Dasgupta, and A. Mookerjee, Phys. Rev. B **50**, 13267 (1994).

[23] A. Alam, S. Ghosh, and A. Mookerjee, Phys. Rev. B **75**, 134202 (2007).

[24] T. L. Swan-Wood, O. Delaire, and B. Fultz, Phys. Rev. B **72**, 024305 (2005).

[25] Quantum-ESPRESSO is a community project for high-quality quantum-simulation software, based on density functional theory, and coordinated by P. Gianozzi. See [http://www.Quantum-Espresso.org] and [http://www.pwscf.org].

[26] S. Baroni, S. De Gironcoli, A. Dal Corso, and P. Giannozzi, Rev. Mod. Phys. **73**, 515 (2001).

[27] D. Vanderbilt, Phys. Rev. B **41**, 7892 (1990); S. G. Louie, S. Froyen, and M. L. Cohen, *ibid.* **26**, 1738 (1982).

[28] M. Methfessel and A. T. Paxton, Phys. Rev. B **40**, 3616 (1989).

[29] A. van de Walle, Ph.D. thesis, MIT Press, Cambridge, MA, 2000.

[30] P. Biswas, B. Sanyal, M. Fakhruddin, A. Halder, A. Mookerjee, and M. Ahmed, J. Phys.: Condens. Matter **7**, 8569 (1995).

[31] K. K. Saha, T. Saha-Dasgupta, A. Mookerjee, and I. Dasgupta, J. Phys.: Condens. Matter **16**, 1409 (2004).

[32] J.-O. Andersson and B. Sundman, CALPHAD: Comput. Coupling Phase Diagrams Thermochem. **11**, 83 (1987).

[33] M. S. Lucas, A. Papandrew, B. Fultz, and M. Y. Hu, Phys. Rev. B **75**, 054307 (2007).